engineering proceedings

MDPI

Proceeding Paper

On the Sensitivity of Potential Evapotranspiration in Egypt to Different Dynamical Downscaling Options and Boundary Layer Schemes Using a High-Resolution Regional Climate Model †

Samy Ashraf Anwar [1,*] and Ankur Srivastava [2,*]

[1] Egyptian Meteorological Authority, Qobry EL-Kobba, Cairo P.O. Box 11784, Egypt
[2] Faculty of Science, University of Technology Sydney, Sydney P.O. Box 2006, Australia
* Correspondence: ratebsamy@yahoo.com (S.A.A.); ankursrivastava117@gmail.com (A.S.)
† Presented at the 4th International Electronic Conference on Applied Sciences, 27 October–10 November 2023; Available online: https://asec2023.sciforum.net/.

Abstract: Accurate information on potential evapotranspiration (PET) is mandatory for arid regions (such as Egypt) to assess crop water requirements. Such precision is limited by the dynamical downscaling options and the physical settings used in regional climate models (like the RegCM4). To address these issues, four simulations were run as part of the current study. The first two simulations take direct (DIR) and one-way nesting (NEST) into account, while the other two use two boundary layer techniques (HOLTSLAG; HOLT) and (the University of Washington; UW). All simulations were driven via an ERA-Interim reanalysis of 1.5 degrees. The simulated PET was evaluated for the high-resolution reanalysis gridded derived product of ERA5-Land (hereafter ERA5). The findings revealed no discernible difference between DIR and NEST regarding global incident solar radiation (RSDS). Also, NEST had a higher mean air temperature (TMP) than DIR. Additionally, UW had a lower TMP than HOLT, but switching between HOLT and UW did not significantly impact the simulated RSDS. Concerning PET, it is neither affected by DIR and NEST nor HOLT and UW. Such results suggest that the RSDS is the main driver in controlling PET variability, followed by TMP. Therefore, by using the DIR downscaling option and UW boundary layer scheme throughout the period of 1990–2020, as recommended by the World Meteorological Organization, the RegCM4 can be used to develop a regional PET map of Egypt.

Keywords: DIR; NEST; HOLT; regional climate model; PET

Citation: Anwar, S.A.; Srivastava, A. On the Sensitivity of Potential Evapotranspiration in Egypt to Different Dynamical Downscaling Options and Boundary Layer Schemes Using a High-Resolution Regional Climate Model. *Eng. Proc.* **2023**, *56*, 116. https://doi.org/10.3390/ASEC2023-15357

Academic Editor: Simeone Chianese

Published: 8 December 2023

1. Introduction

The Fourth Assessment Report of the Intergovernmental Panel on Climate Change (IPCC; [1]) reported that both the Middle East and North Africa (MENA, as a hot-spot water-scarce region) shows a high rate of water need (represented by potential evapotranspiration (PET)) as a result of mean air temperature increase particularly under the Representative Concentration Pathway 8.5 (RCP8.5). Although the Penman-Monteith equation (PM; [2]) has been recommended to compute PET because it is based on physical principles governing the physical exchange of water and energy between the surface and atmosphere, it requires many atmospheric variables (most of them are calculated empirically, leading to a large increase in the uncertainty of the computed PET as reported by [3]). Instead, the Hargreaves-Samani equation (HS; [4]) has been used to compute PET. The HS equation has several advantages; for example, it is recommended to be calculated directly after the PM equation [5], and it provides an easy way to track future projected PET changes (as a function of mean air temperature) under different future scenarios [3].

The construction of a regional PET map (either in the present climate or under different future scenarios) can be carried out by using high−resolution regional climate models (RCMs such as the RegCM4 [6]). Additionally, the accurate estimation of atmospheric

variables (especially those involved in computing PET) can be ensured by investigating different options of dynamical downscaling or various combinations of physical schemes (e.g., boundary layer). For instance, the authors of [7] reported that high-resolution RCMs and improved physical parameterization could ensure a high capability to reproduce large-scale atmospheric circulations. The authors of [8] also conducted experiments to constrain the mean air temperature and total surface precipitation concerning different reanalysis products using the RegCM4. They reported that direct downscaling to high-resolution ensures better performance than adopting a one-way nesting technique.

In Egypt, the author of [9] examined the role of boundary layer schemes in constraining the daily mean air temperature using the RegCM4. They reported that the University of Washington scheme (UW [10]) is better at simulating the mean air temperature than the HOLTSLAG (HOLT [11]) for the ERA5 reanalysis product. Additionally, the authors of [9] observed that the global incident solar radiation was affected neither by the options of dynamical downscaling (direct or one-way nesting) nor by the boundary layer schemes (HOLT or UW). However, the influence of different options of dynamical downscaling or boundary layer schemes on the simulated PET of Egypt was not examined in this study. Therefore, the target of the present study is to:

1. Examine the influence of dynamical downscaling options (direct versus one-way nesting) and boundary layer schemes (HOLT versus UW) on the simulated PET in comparison with the ERA5 reanalysis product as the ground truth of observations of PET.
2. Examine the dependence of the simulated PET on the global incident solar radiation and daily mean air temperature (as inputs of the HS equation) by constructing a regional map of the Pearson correlation coefficient in each case. The significant correlation was calculated using Student's *t*-test with alpha equal to 5%.
3. Investigate the performance of the RegCM4 concerning the climatological annual cycle of PET concerning ERA5 for ten locations representing different climate zones of Egypt (see Section 3).

Section 2 describes the study area and experiment design; Section 3 shows the results. Section 4 provides the discussion and conclusion.

2. Materials and Methods

2.1. Study Area

Egypt (an important country in the MENA region) is bordered by the Mediterranean Sea in the north and the Red Sea in the east. From a climatic point of view, Egypt is categorized as a semi-arid region. According to the Köppen climate classification, Egypt is classified as a desert climate. The maximum and annual values of relative humidity vary within the study region. For example, Cairo has minimum values during spring (around 48%) and maximum values in summer (about 70%). Also, Egypt is characterized by heatwaves during the spring and summer seasons (intense in Upper Egypt and moderate on the northern coast).

The dominant wind direction of the coast of the Mediterranean Sea is northwest, which can explain the moderate temperature in this region. In Upper Egypt (Aswan, Luxor, Asyut, or Sohag), the nighttime temperatures become high, especially in the summer (average high temperatures exceed 40 °C). In addition, the high elevation topography (e.g., Saint Catherine Mountains) plays an important role in controlling the nighttime temperature [12].

2.2. Experiment Design

In the present study, we used the fourth generation of the RegCM regional climate model (the RegCM4 [6]). The RegCM4 has been used to compute PET in regions such as Bulgaria [3]. Four experiments were conducted over the period 1997–2017 to address the influence of different options of dynamical downscaling and boundary layer schemes on the simulated PET. The first year was considered as a spin-up to initialize the RegCM4 with an equilibrium state of the atmosphere [13]; hence, the analysis starts in 1998 and ends in

2017. The RegCM4 was downscaled in all simulations via the ERA-Interim reanalysis of 1.5 degrees (EIN15 [14]). The present study customized the RegCM4's domain with 25 km horizontal resolution with 60 grid points in both zonal and meridional directions. Figure 1 shows the surface elevation of Egypt (in meters), including the ten locations.

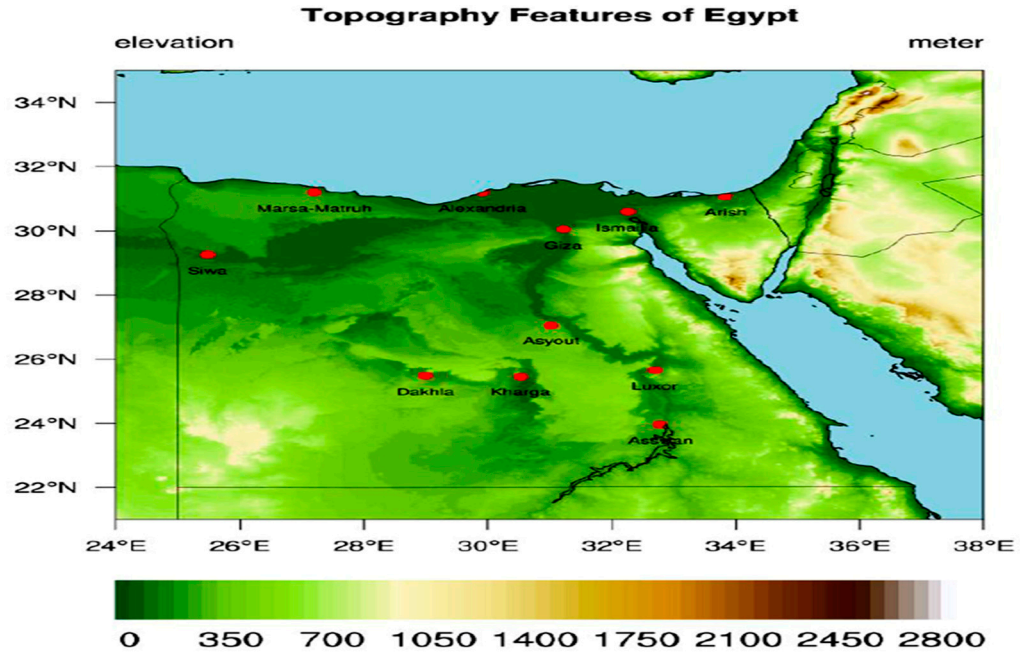

Figure 1. Surface elevation of Egypt (in meters). The red dots indicate the location of stations reported in the present study.

The four simulations were grouped into two cases to serve the purpose of the present study. The first case considers the dynamical downscaling options direct (DIR) and one-way nesting (NEST) following [9]. However, the second case manipulates the boundary layer schemes HOLT and UW as in [9]. PET was calculated using a calibrated version of the HS equation following [15] in the four simulations. The simulated PET was evaluated for the derived ERA5-land reanalysis product [16]. In addition, significant differences between the two simulations (of each case) were calculated using Student's *t*-test with alpha equal to 5%. Figure S1 shows a methodological flowchart summarizing the steps of the present study. In the present study, the simulated PET was calculated using a calibrated version of the HS equation [15]. The calibrated HS equation can be written as:

$$PET_{HS} = 0.0105 \times RSDS \times (TMP + 17.8),$$

where RSDS is the global incident solar radiation (in mm day^{-1} to match the PET unit [2]) and TMP is the 2 m mean air temperature (in °C).

2.3. Validation Data

The authors of [15] reported that the long-term records of station PET data may not be available spatially or temporally. However, a new high-resolution gridded PET reanalysis product (hPET [17]) was developed. This product computes PET using the PM equation and retrieves the meteorological variables (involved in computing PET) from the ERA5-land product [16]. The hPET product was originally available in 0.1 degrees for 40 years (1981–2021) in hourly time scales and daily sums.

According to [17], hPET shows good consistency with the available global PET products, particularly Climate Research Unit (CRU [18]). Additionally, hPET products can be used in ecohydrology and drought propagation. Recently, the hPET was used to assess the RegCM4's performance [15]. For the present study, all products were bilinearly interpolated on the RegCM4 curvilinear grid [3].

3. Results

The authors of [15] claimed that calibrating the global incident solar radiation's coefficient (RSDS) is more efficient than the one of the daily mean air temperature (TMP). Because the simulated PET is affected by both the RSDS and TMP [3,4], it is important to investigate the influence of dynamical downscaling and boundary layer options to explain the observed changes in the simulated PET in each case. The authors of [9] reported that dynamical downscaling (DIR or NEST) has an insignificant impact on the simulated RSDS in all seasons.

Switching between DIR and NEST considerably affects the simulated TMP through changes in the ground temperature and sensible heat flux (as NEST amplifies the positive bias compared to the DIR). For the boundary layer parameterization, the authors of [9] noted that the UW has a lower TMP than the HOLT, particularly for spring and winter seasons. Moreover, the simulated RSDS does not change in the transition between HOLT and UW.

3.1. Seasonal Climatology

3.1.1. Influence of Dynamical Downscaling Options on PET

Figure 2 shows a comparison between DIR and NEST concerning the ERA5 reanalysis product and the difference between NEST and DIR. In general, it can be observed that the RegCM4 can reproduce the spatial pattern of the simulated PET for ERA5, as PET shows minimum values in the winter season (December−January−February; (DJF); Figure 2s−u) followed by the spring (March−April−May; (MAM); Figure 2a–c) than summer (June−July−August; (JJA); Figure 2g–l), and, finally, autumn (September−October−November; (SON); Figure 2m–o). DIR and NEST also show a negative PET bias of 1–2 mm day^{-1} in the MAM and JJA seasons (Figure 2d,e,j,k). Meanwhile, both simulations show a positive bias of 1–2.5 mm day^{-1} in the SON season. Finally, in the DJF season, the RegCM4 bias approaches its minimum value (around +0.5 mm day^{-1}; Figure 2v,w). Qualitatively, no observed difference is noted between the two simulations in all seasons (see Figure 2f,l,r,x).

3.1.2. Influence of Boundary Layer Schemes on PET

Figure 3 shows the simulated PET of the HOLT and UW compared to ERA5 and the difference between the HOLT and UW. Similar to Figure 2, the RegCM4 successfully captures the spatial pattern of PET concerning the ERA5 product in all seasons (Figure 3a–c,g–i,m–o,s–u). Additionally, the RegCM4 bias is similar to the one noted in the case of dynamical downscaling in all seasons (Figure 3d,e,j,k,p,q,v,w). Lastly, the two simulations have no considerable difference in all seasons (see Figure 3f,l,r,x).

From Figures 2 and 3, one can observe that the simulated PET is sensitive neither to the option of dynamical downscaling (DIR/NEST) nor the boundary layer parameterization, despite the noted changes in the TMP in both cases [9]. This noted behavior can be attributed to the fact that the RSDS is not affected by dynamical downscaling and boundary layer options. Therefore, the RSDS mainly controls PET, which will be further discussed in Section 3.2.

3.2. Dependence of PET on RSDS and TMP

In Section 3.1, it was observed that the RSDS is the main driver of PET changes followed by the TMP. To confirm this point, a regional map of the Pearson correlation coefficient was plotted between PET, RSDS, and TMP for each case. Significant correlation was calculated using Student's *t*-test with alpha equals to 5%. Figure 4 shows the correlation between PET and TMP (Figure 4a), while the correlation between PET and RSDS concerning the DIR simulation is indicated in Figure 4b.

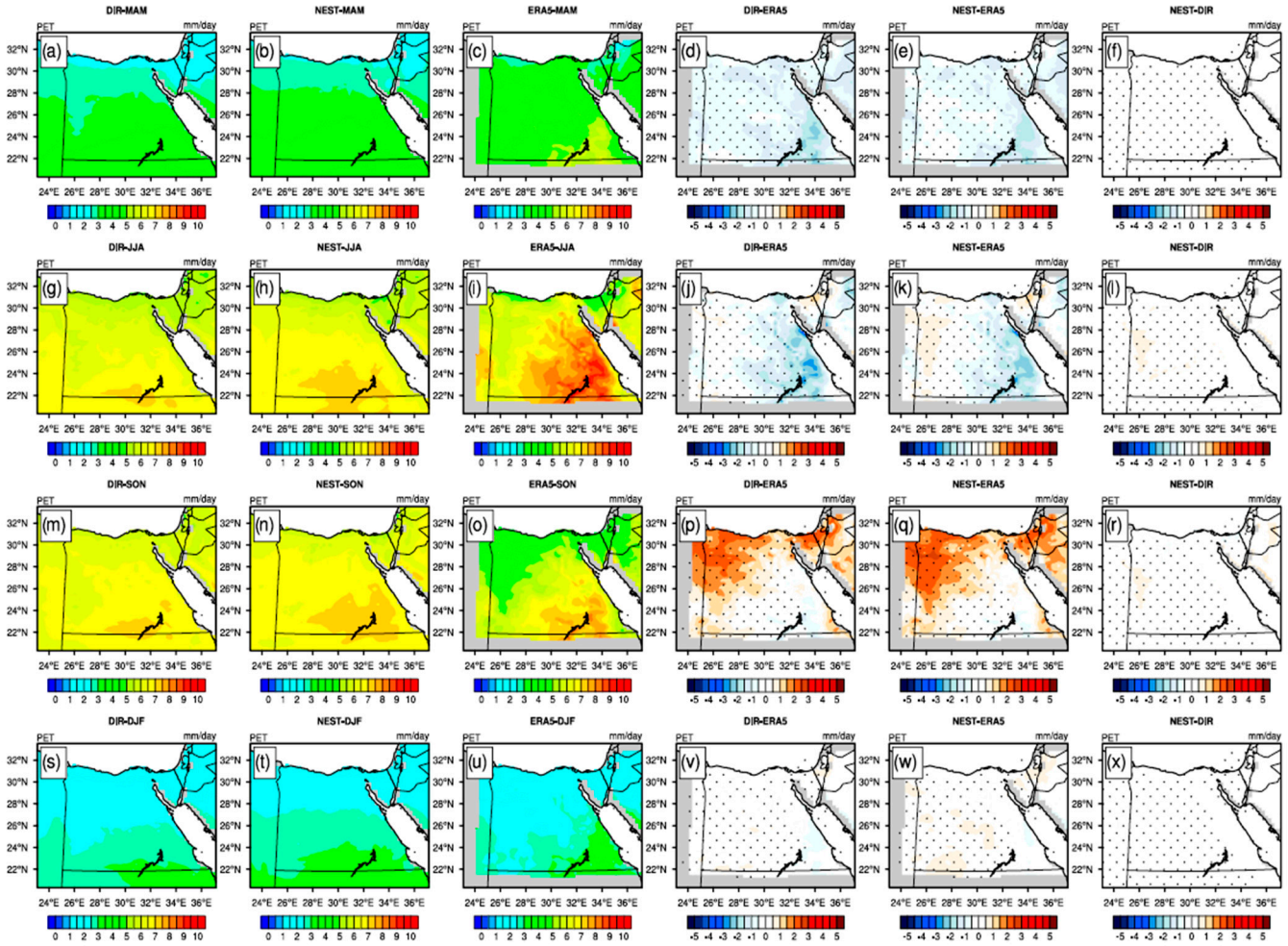

Figure 2. The potential evapotranspiration over the period 1998–2017 (PET; in mm day^{-1}) for MAM season in the first row (**a**–**f**); JJA in the second row (**g**–**l**); SON in the third row (**m**–**r**); and DJF in the fourth row (**s**–**x**). For each row, DIR is on the left, followed by NEST; ERA5 is third from left, DIR minus ERA5, NEST minus ERA5, and the difference between NEST and DIR. Significant difference/bias is indicated via black dots using Student's *t*-test with alpha equal to 5%.

Figure 4a shows that the correlation between PET and TMP exhibits a gradient that differs with the examined region. For instance, in the 30–32° N region, the PET–TMP correlation gradient ranges between 0.9 and 0.94. Meanwhile, in the 22–28° N region, the correlation ranges between 0.94 and 0.96. For the PET–RSDS dependence, it can be noted that the correlation is between 0.96 and 0.98 (Figure 4c). In the NEST simulation, the PET–TMP dependence is quite different from the one observed in the DIR simulation because NEST is warmer than DIR in all seasons [9]. This point can be confirmed by noting that the correlation in this case ranges between 0.9 and 0.95 (Figure 4c). For the RSDS, the situation is not quite different from the DIR simulation because RSDS does not change between the two simulations. Therefore, it can be observed that the correlation ranges from 0.96 to 0.98 similar to the DIR simulation (Figure 4d).

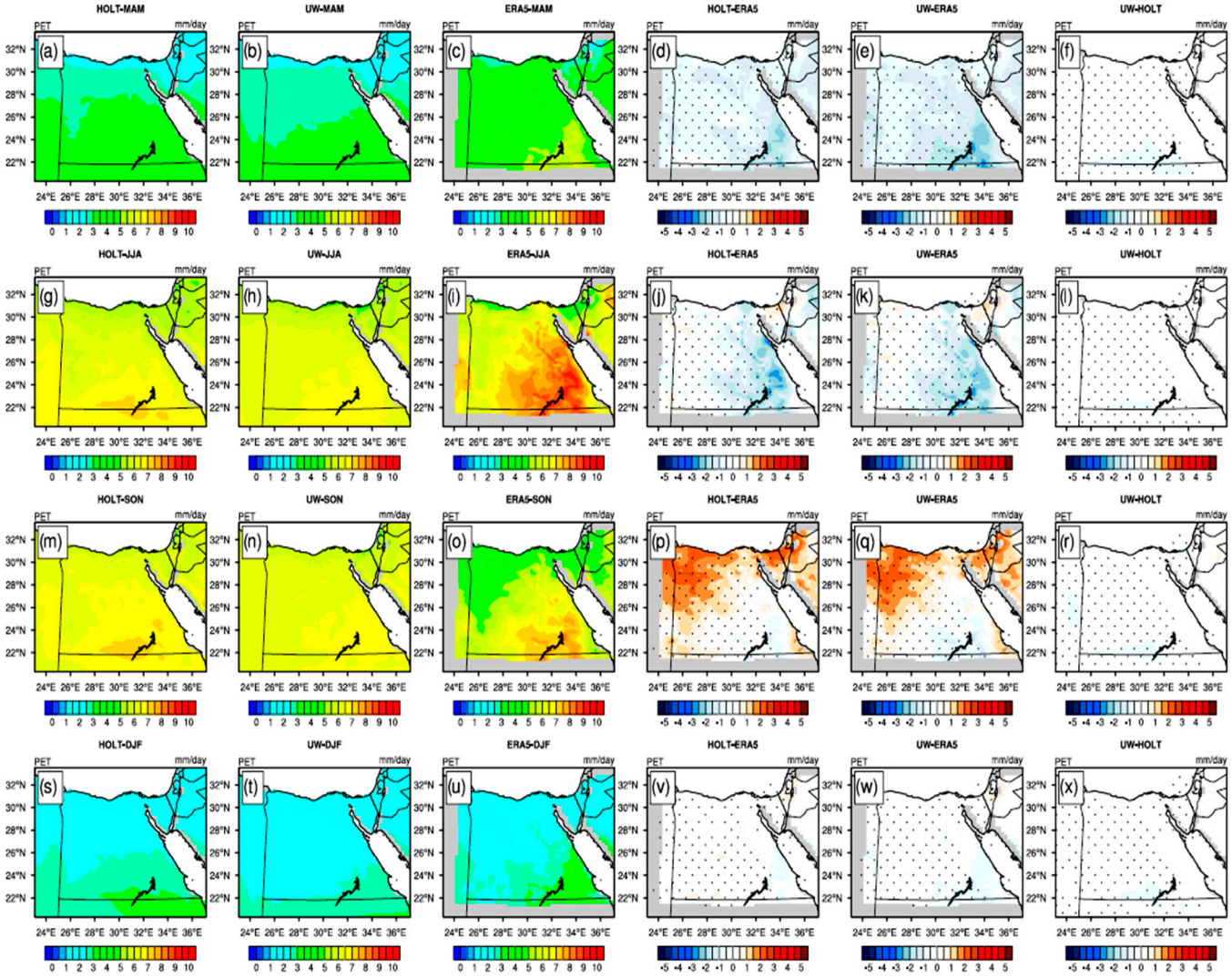

Figure 3. The potential evapotranspiration over the period 1998–2017 (PET; in mm day^{-1}) for MAM season in the first row (**a**–**f**); JJA in the second row (**g**–**l**); SON in the third row (**m**–**r**); and DJF in the fourth row (**s**–**x**). For each row, HOLT is on the left, followed by UW; ERA5 is third from left, HOLT minus ERA5, UW minus ERA5, and the difference between UW and HOLT. Significant difference/bias is indicated via black dots using Student's *t*-test with alpha equal to 5%.

Moving to the boundary layer case, the PET–TMP correlation does not vary much between the boundary layer schemes (see Figure 5a,c) compared to the case of dynamical downscaling. For example, the correlation (in the two simulations, HOLT and UW) ranges between 0.9 and 0.96. This noted behavior can be attributed to two reasons: (1) the difference between DIR and NEST is larger than HOLT and UW and (2) regarding TMP changes between HOLT and UW, RSDS is the main driver of PET changes followed by TMP. Regarding RSDS, there is only a 1% difference between the correlations of the two simulations. For instance, for the HOLT simulation (Figure 5c), the correlation ranges between 0.96 and 0.98. However, the correlation lies between 0.95 and 0.98 for the UW simulation (Figure 5d).

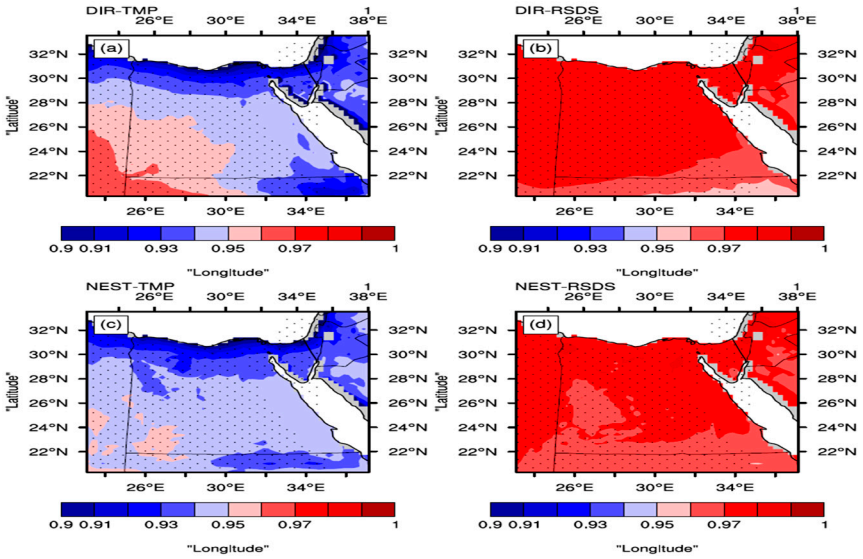

Figure 4. The Pearson correlation coefficient for each grid point for: DIR ((**a**) for TMP, and (**b**) for RSDS), and NEST ((**c**) for TMP and (**d**) for RSDS). Note that the range of 0.9 and 1 was chosen after many trials to choose the appropriate range.

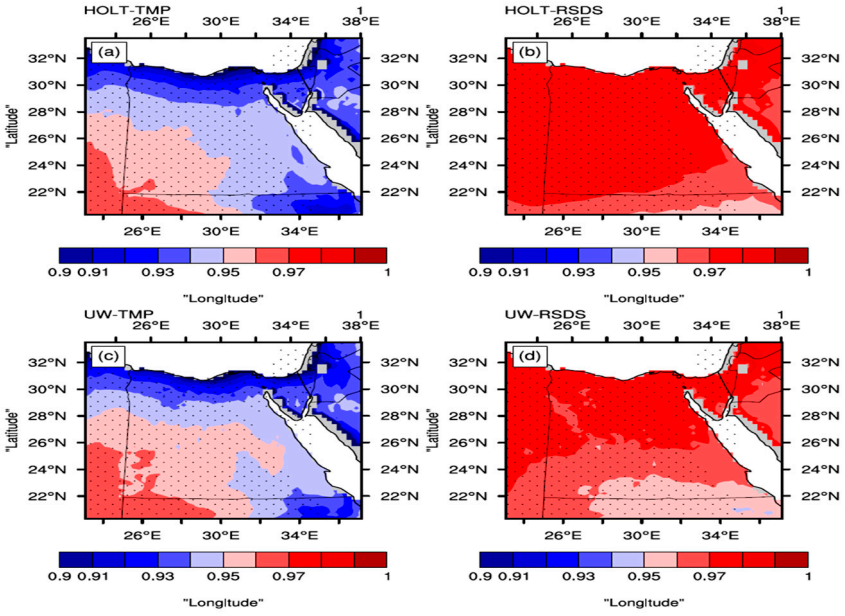

Figure 5. The Pearson correlation coefficient for each grid point for: HOLT ((**a**) for TMP), and (**b**) for RSDS), and UW ((**c**) for TMP and (**d**) for RSDS). Note that the range of 0.9 and 1 was chosen after many trials to choose the appropriate range.

3.3. Climatological Annual Cycle of PET

The combination of DIR–UW (the RegCM4) was considered based on the recommendation of [9]. The climatological annual cycle of the PET was evaluated for ERA5. Preliminary analysis indicated that the simulated PET annual cycle can be categorized as: phase (Figure 6) and non-phase (Figure 7) shifts. In the phase shift, the simulated PET maximum value is either delayed or advanced concerning ERA5. However, the non-phase-shift considers consistency in the PET maximum value between the RegCM4 and ERA5. Each phase comprises five stations. For instance, Figure 6 shows the annual cycle of the simulated PET (in comparison with ERA5) for the following locations: Alexandria, Arish, Giza, Ismaila, and Siwa.

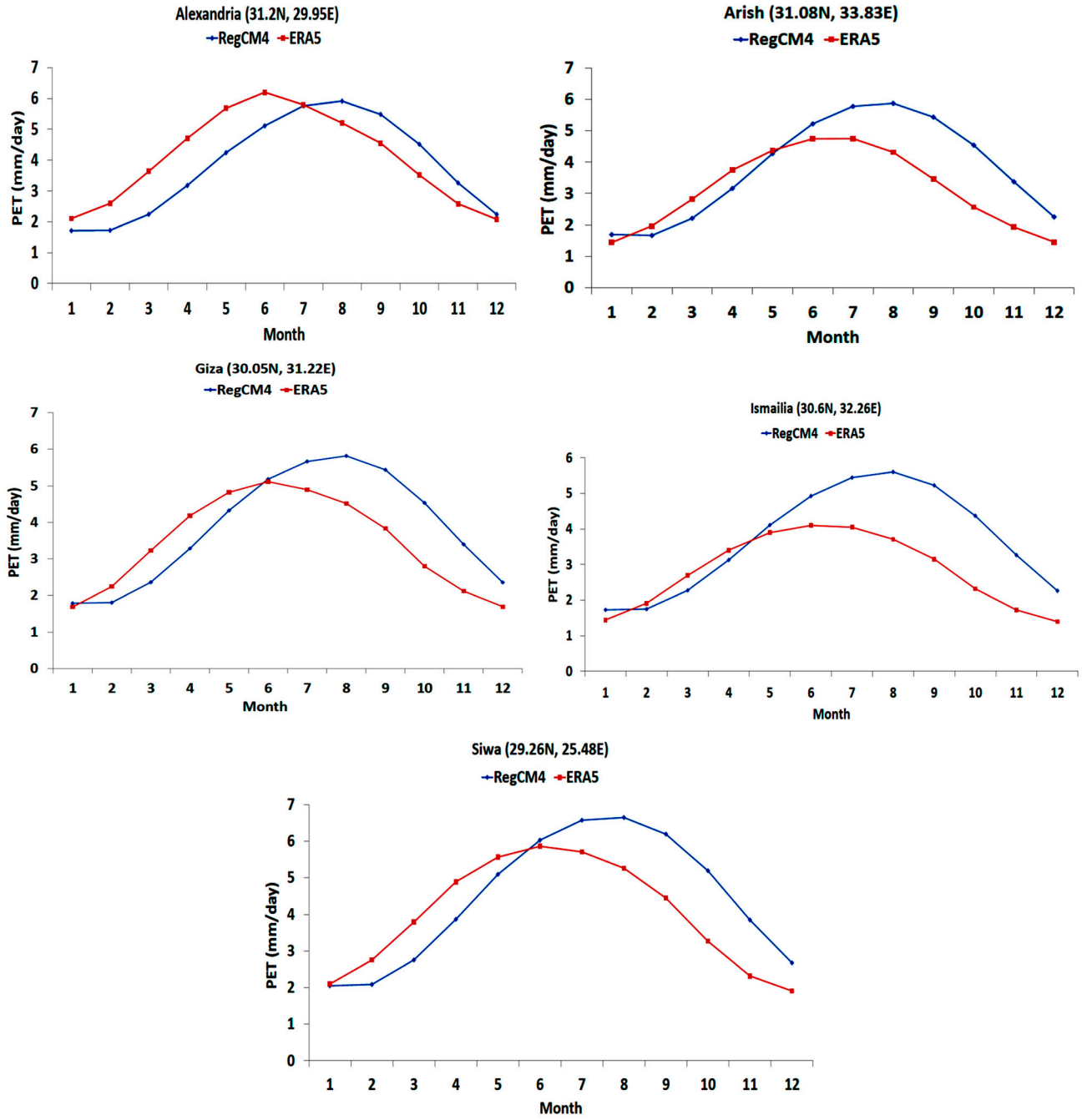

Figure 6. The climatological annual cycle of the simulated PET for ERA5 for the following locations: Alexandria, Arish, Giza, Ismaila and Siwa.

However, Figure 7 considers the comparison between the simulated PET and ERA5 for the following locations: Asswan, Asyout, Dakhla, Kharga and Luxor. Figure 6 shows that the RegCM4 underestimates PET (from January to June) while it overestimates the PET during the rest of the months in Alexandria. Additionally, RegCM4's peak occurs in August, and ERA5's peak occurs in June. The four locations (Arish, Giza, Ismailia, and Siwa) share a common feature regarding RegCM4's behavior concerning ERA5. For instance, in the aforementioned locations, the RegCM4 is close to ERA5 from January to May, while the RegCM4 overestimates PET during the rest of the months. Like Alexandria, the RegCM4's peak occurs in August, while ERA5 peaks in June. In Giza, RegCM4's peak occurs in July and August, while the ERA5 peaks in June and July.

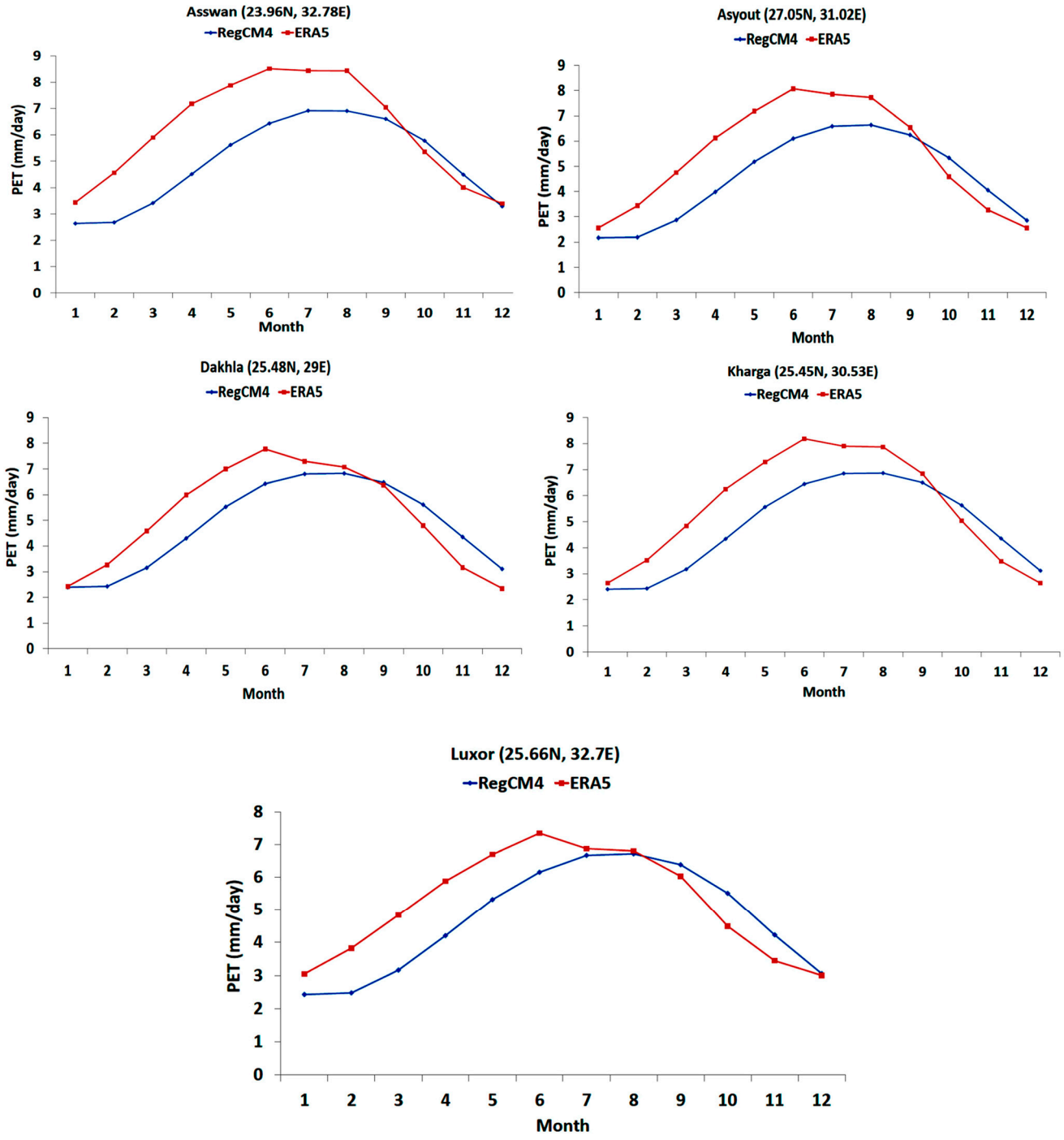

Figure 7. The climatological annual cycle of the simulated PET for ERA5 for the following locations: Asswan, Asyout, Dakhla, Kharga and Luxor.

From Figure 6, it can be observed that the RegCM4 has a limited ability to reproduce the climatological annual cycle of the simulated PET with ERA5 for the coastal locations (Alexandria, Arish, Ismailia and Siwa) and near-coast location (Giza). In Figure 7, the situation is different because the RegCM4 can reproduce the simulated annual cycle of PET compared to ERA5. For instance, the RegCM4 and ERA5 show the PET peak during June, July, and August. Additionally, the RegCM4 underestimates PET from January to August, while the RegCM4 is close to ERA5 during the rest of the months.

4. Discussion and Conclusions

The accuracy of estimating potential evapotranspiration (PET) is a mandatory requirement for a proper assessment of crop water needs and the monitoring of agricultural and meteorological droughts. To achieve this accuracy, the authors of [2] recommended the PM equation to estimate PET. However, the PM equation is data-intensive, requiring many atmospheric variables that are not available spatially/temporally [19]. Hence, there is an urgent need to estimate PET using a simple empirical method with a minimum number of meteorological inputs [3,4]. However, the original version of the empirical equation may not be suitable for estimating PET, causing over/underestimation of the PM observations. Therefore, local calibration (according to the study region) can give reasonable accuracy in estimating PET.

Focusing on the HS equation (the alternative model of the PM), the calibration has proven its efficiency in various regions across the globe, such as Egypt [15], Bulgaria [3], Sudan and South Sudan [5], West Texas [19], and Nigeria [20]. Additionally, the accuracy of the calculated PET is affected by the configuration of the regional climate model (e.g., the RegCM4) used for this purpose. The authors of [8] used the RegCM4 to conduct two experiments: (1) studying the influence of the direct down-scaling of ERA-Interim reanalysis with different horizontal grid spacings and (2) making a comparison between direct down-scaling and two-way nesting using ERA-Interim of 1.5 degrees on the near daily average air temperature and total surface precipitation. They claimed that the accuracy of the RegCM4 can be improved when direct down-scaling with an acceptable resolution is adopted.

In Egypt, the accuracy of the RegCM4 has been examined via various boundary layer schemes [9]. In this study, the authors reported that the UW scheme is better than the HOLT scheme in simulating daily mean air temperature concerning ERA5. However, the influence of dynamical downscaling options or the role of the boundary layer schemes has not been examined for the PET of Egypt until now.

The present study addressed the influence of dynamical downscaling and boundary layer options by conducting four simulations with a 25 km horizontal grid from 1997 to 2017. Also, the simulated PET was calculated using a calibrated version of the HS following [15]. The high−resolution global gridded PET product (hPET) was used as the benchmark for evaluating the simulated PET. The results of this study can be summarized in the following points:

1. The simulated PET is insensitive to the dynamical downscaling and boundary layer options, despite the noted changes of TMP [9].
2. RSDS is the main driver of PET changes, followed by the TMP.
3. On a point-scale, the simulated climatological annual cycle of PET is categorized as phase and non-phase shift.

In conclusion, the RegCM4 can be used to develop a PET map of Egypt using the DIR-UW configuration. This finding not only aids policy makers in assessing the daily water requirements of crops, which is crucial for daily forecasts, especially in regions with limited data, but also holds the potential for projecting future water needs under varying warming scenarios. Such insights provide a vital resource for strategic decision-making in agricultural and water resource management, offering a bridge between scientific advancements and actionable policies.

It is worth mentioning that the present study did not consider the influence of aerosols on the RSDS budget, and ultimately, the simulated PET. Also, long term in-situ observations were not available during the time of the experiment. Instead, we used hPET to evaluate the performance of the RegCM4 on a point scale. Additionally, bias-correction techniques (e.g., [12]) have not been applied to correct the RegCM4 output of each season. Finally, the present study relies on using one regional climate model (RCM). In a future study, the following points will be addressed:

1. The influence of aerosols will be considered to address the noted changes in RSDS, TMP, and PET.
2. The sensitivity of the simulated PET to different lateral boundary conditions (adopted from the General Circulation Models participating in the Fifth Coupled Model Intercomparison Project—CMIP5; [21]) will be studied by examining the simulated RSDS and TMP.

Supplementary Materials: The following supporting information can be downloaded at: https://www.mdpi.com/article/10.3390/ASEC2023-15357/s1, Figure S1: A methodological flowchart summarizing the steps of the present study.

Author Contributions: Conceptualization, S.A.A.; methodology, S.A.A.; software, S.A.A.; validation, S.A.A.; formal analysis, S.A.A. and A.S.; investigation, S.A.A. and A.S.; resources, S.A.A.; data curation, S.A.A.; writing—original draft preparation, S.A.A. and A.S.; writing—review and editing, S.A.A. and A.S.; visualization, S.A.A.; supervision, S.A.A. and A.S.; project administration, S.A.A. All authors have read and agreed to the published version of the manuscript.

Funding: This research received no external funding.

Institutional Review Board Statement: Not applicable.

Informed Consent Statement: Not applicable.

Data Availability Statement: Data are contained within the article.

Acknowledgments: The Egyptian Meteorological Authority (EMA) is acknowledged for providing the computational power to conduct the model simulations. Hourly potential evapotranspiration (hPET) was retrieved from the web link https://data.bris.ac.uk/data/dataset/qb8ujazzda0s2aykkv0oq0ctp (accessed on 18 October 2022). However, the authors can acquire the monthly mean upon request. Finally, we would like to thank Shabnam Pourshirazi (from the Gorgan University of Agricultural Sciences & Natural Resources Gorgan, Iran) for her efforts to improve the manuscript quality.

Conflicts of Interest: The authors declare no conflict of interest.

References

1. IPCC. *Climate Change 2007: Synthesis Report*; Technical report; IPCC: Geneva, Switzerland, 2007.
2. Allen, G.R.; Pereira, S.L.; Raes, D.; Smith, M. *Crop Evapotranspiration: Guidelines for Computing Crop Water Requirements*; Report 56; Food and Agricultural Organization of the United Nations (FAO): Rome, Italy, 1998; 300p.
3. Anwar, S.A.; Malcheva, K.; Srivastava, A. Estimating the potential evapotranspiration of Bulgaria using a high-resolution regional climate model. *Theor. Appl. Climatol.* **2023**, *152*, 1175–1188. [CrossRef]
4. Hargreaves, G.L.; Allen, R.G. History and evaluation of Hargreaves evapotranspiration equation. *J. Irrigat. Drain. Eng.* **2003**, *129*, 53–63. [CrossRef]
5. Elagib, N.A.; Musa, A.A. Correcting Hargreaves-Samani formula using geographical coordinates and rainfall over different timescales. *Hydrol. Process.* **2023**, *37*, e14790. [CrossRef]
6. Giorgi, F.; Coppola, E.; Solmon, F.; Mariotti, L.; Sylla, M.B.; Bi, X.; Elguindi, N.; Diro, G.T.; Nair, V.; Giuliani, G.; et al. Brankovic. RegCM4: Model description and preliminary tests over multiple CORDEX domains. *Clim. Res.* **2012**, *52*, 7–29. [CrossRef]
7. Chen, L.; Huang, G.; Wang, X. Projected changes in temperature, precipitation, and their extremes over China through the RegCM. *Clim. Dyn.* **2019**, *53*, 5859–5880. [CrossRef]
8. Xu, X.; Huang, A.; Huang, Q.; Zhang, Y.; Wu, Y.; Gu, C.; Cai, S.; Zhu, X. Impacts of horizontal resolution of the lateral boundary conditions and downscaling method on the performance of RegCM4.6 in simulating the surface climate over central-eastern China. *Earth Space Sci.* **2022**, *9*, e2022EA002433. [CrossRef]
9. Anwar, S.A.; Mostafa, S.M. On the Sensitivity of the Daily Mean Air Temperature of Egypt to Boundary Layer Schemes Using a High-Resolution Regional Climate Model (RegCM4). *J. Biomed. Res. Environ. Sci.* **2023**, *4*, 474–484. [CrossRef]
10. Grenier, H.; Bretherton, C.S. A moist PBL parameterization for large scale models and its application to subtropical cloud topped marine boundary layers. *Mon. Weather Rev.* **2001**, *129*, 357–377. [CrossRef]
11. Holtslag, A.A.M.; Boville, B.A. Local versus nonlocal boundary layer diffusion in a global model. *J. Clim.* **1993**, *6*, 1825–1842. [CrossRef]
12. Mostafa, S.M.; Anwar, S.A.; Zakey, A.S.; Wahab, M.M.A. Bias-correcting the maximum and minimum air temperatures of Egypt using a high-resolution Regional Climate Model (RegCM4). *Eng. Proc.* **2023**, *31*, 73. [CrossRef]

13. Steiner, A.L.; Pal, J.S.; Rauscher, S.A.; Bell, J.L.; Diffenbaugh, N.S.; Boone, A.; Sloan, L.C.; Giorgi, F. Land surface coupling in regional climate simulations of the West African monsoon. *Clim. Dyn.* **2009**, *33*, 869–892. [CrossRef]
14. Dee, D.P.; Uppala, S.M.; Simmons, A.J.; Berrisford, P.; Poli, P.; Kobayashi, S.; Andrae, U.; Balmaseda, M.A.; Balsamo, G.; Bauer, P.; et al. The ERA-Interim reanalysis: Configuration and performance of the data assimilation system. *Q. J. R. Meteorol. Soc.* **2011**, *137*, 553–597. [CrossRef]
15. Anwar, S.A.; Lazić, I. Estimating the Potential Evapotranspiration of Egypt Using a Regional Climate Model and a High-Resolution Reanalysis Dataset. *Environ. Sci. Proc.* **2023**, *25*, 29. [CrossRef]
16. Singer, M.; Asfaw, D.; Rosolem, R.; Cuthbert, M.O.; Miralles, D.G.; MacLeod, D.; Michaelides, K. Hourly potential evapotranspiration (hPET) at 0.1degs grid resolution for the global land surface from 1981-present. *Sci. Data* **2021**, *8*, 224. [CrossRef] [PubMed]
17. Muñoz-Sabater, J.; Dutra, E.; Agustí-Panareda, A.; Albergel, C.; Arduini, G.; Balsamo, G.; Boussetta, S.; Choulga, M.; Harrigan, S.; Hersbach, H.; et al. ERA5-Land: A state-of-the-art global reanalysis dataset for land applications. *Earth Syst. Sci. Data* **2021**, *13*, 4349–4383. [CrossRef]
18. Harris, I.; Osborn, T.J.; Jones, P.; Lister, D. Version 4 of the CRU TS monthly high-resolution gridded multivariate climate dataset. *Sci. Data* **2020**, *7*, 109. [CrossRef]
19. Awal, R.; Rahman, A.; Fares, A.; Habibi, H. Calibration and Evaluation of Empirical Methods to Estimate Reference Crop Evapotranspiration in West Texas. *Water* **2022**, *14*, 3032. [CrossRef]
20. Ogunrinde, A.T.; Emmanuel, I.; Enaboifo, M.A.; Ajayi, T.A.; Pham, Q.B. Spatio-temporal calibration of Hargreaves–Samani modeling the Northern Region of Nigeria. *Theor. Appl. Climatol.* **2022**, *147*, 1213–1228. [CrossRef]
21. Taylor, K.E.; Stoufer, R.J.; Meehl, G.A. An overview of CMIP5 and the experiment design. *Bull. Am. Meteorol. Soc.* **2012**, *90*, 485–498. [CrossRef]